Molecular modeling and experimental study of non-linear optical compounds: Monosubstituted derivatives of dicyanovinylbenzene

ARTICLE *in* JOURNAL OF MOLECULAR STRUCTURE · FEBRUARY 2000

Impact Factor: 1.6 · DOI: 10.1016/S0022-2860(99)00305-1

ELSEVIER

Journal of Molecular Structure 519 (2000) 225–241

Journal of
MOLECULAR
STRUCTURE

www.elsevier.nl/locate/molstruc

Molecular modeling and experimental study of non-linear optical compounds: monosubstituted derivatives of dicyanovinylbenzene

T.V. Timofeeva[a,*], V.N. Nesterov[b], M.Yu. Antipin[a,b], R.D. Clark[a], M. Sanghadasa[c], B.H. Cardelino[d], C.E. Moore[e], D.O. Frazier[e]

[a]*Department of Physical Sciences, New Mexico Highlands University, Las Vegas, NM 87701, USA*
[b]*Institute of Organoelement Compounds, Russian Academy of Sciences, 28 Vavilov St., B-334, Moscow, Russian Federation*
[c]*University of Alabama in Huntsville, Huntsville, AL 35899, USA*
[d]*Chemistry Department, Spelman College, Atlanta University Center, Atlanta, GA 30314, USA*
[e]*Space Science Laboratory, NASA George C. Marshall Space Flight Center, Huntsville, AL 35812, USA*

Received 13 April 1999; accepted 9 June 1999

Abstract

A search for potential non-linear optical (NLO) compounds has been performed using the Cambridge Structural Database and molecular modeling. We have studied a series of monosubstituted derivatives of dicyanovinylbenzene as the NLO properties of one of its derivatives (*o*-methoxy-dicyanovinylbenzene, DIVA) were described earlier. The molecular geometry in the series of the compounds studied was investigated with an X-ray analysis and discussed along with results of molecular mechanics and ab initio quantum chemical calculations. The influence of crystal packing on the molecular planarity has been revealed. Two new compounds from the series studied were found to be active in the second harmonic generation (SHG) in the powder state. The measurements of the SHG efficiency have shown that the *o*-F-, and *p*-Cl-derivatives of dicyanovinylbenzene are about 10 and 20 times more active than urea, respectively. The peculiarities of crystal structure formation in the framework of balance between the van der Waals and electrostatic interactions have been discussed. The crystal morphology of DIVA and two new SHG-active compounds have been calculated on the basis of the known crystal structures.

Keywords: Cyanoderivatives; Non-linear optical properties; X-ray analysis; Ab initio calculations

1. Introduction

Organic compounds with non-linear optical (NLO) properties have been under intensive investigation for the last two decades. The main incentive for this is that in many respects organic compounds might be more effective than many well-known inorganic materials. Nevertheless, not all peculiarities of the formation of crystals of organic materials are completely understood. Molecular modeling and structure–property relations for some organic NLO compounds have been described in the literature (see, for example reviews [1,2]), but the interrelations of the molecular and crystal structure are still uncertain in many respects. There have been attempts to find an approach to predict centric/acentric crystal structure for a given compound based on calculation of the most stable molecular dimer associates which have

* Corresponding author. Tel.: + 1-505-454-3362; fax: + 1-505-454-1303.
E-mail address: tanya@mount.nmhu.edu (T.V. Timofeeva).

0022-2860/00/$ - see front matter
PII: S0022-2860(99)00305-1

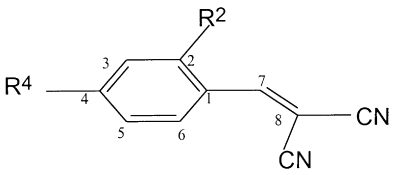

R^2 = H (**I**), F (**II**), Cl (**III**), OMe (**IV**), NO_2 (**V**), NC_4H_8 (**VI**), and R^4= H;

or R^2 = H, and R^4 = Cl (**VII**), OMe (**VIII**), NMe_2 (**IX**), NEt_2 (**X**),

$CH=C(CN)_2$ (**XI**), $(SiH_2)_2C_6H_4NH_2$ (**XII**).

Scheme 1.

given some positive results [3–6], but it was demonstrated [7] that in general this approach may be considered only as feasible one. Recent progress in the prediction of the organic crystal structures is summarized in Refs. [8,9].

In the present paper we have extended the search for new NLO compounds using two novel approaches. First we have modeled, synthesized and investigated compounds whose molecular shape resembles those of compounds with known acentric crystal structure. And second, we have scanned the Cambridge Structural Database (CSD) looking for such compounds in order to obtain information about their crystal structure and to test their NLO properties whenever their crystal structure was acentric.

In the framework of a systematic investigation of new organic NLO compounds, a series of substituted derivatives of dicyanovinylbenzene was considered as a model molecular system (see Scheme 1). We choose these simple molecules in order to find out if there is any relationship between substituent positions in the benzene ring and formation of centrosymmetric or acentric crystals.

X-ray diffraction analysis of compounds **II, III** and **V** has been performed in the present work, crystal structures of compounds **I**, **IV**, **VIII**, **IX**, **X** were described in our previous papers [5,7,10], and the structural information about compounds **III**, **VI**, **VII**, **XI, XII** was found in the Cambridge Structural Database. We combined the information about the crystal structures of the listed compounds with results of their molecular structure calculations as well as polarizability calculations and experimental measurements of the NLO properties. We also modeled and investigated crystal habit for several SHG-active compounds as information on the predominant direction of the crystal growth is very important for film growth and device fabrication.

2. Experimental part and calculation details

2.1. Materials

Synthesis of 2-fluorobenzylidenmalononitrile [2-(2-fluorophenyl)-1,1-dicyanoethylene] (**II**), 2-chlorobenzylidenmalononitrile [2-(2-chlorophenyl)-1,1-dicyanoethylene] (**III**), 2-nitrobenzylidenmalononitrile [2-(2-chlorophenyl)-1,1-dicyanoethylene] (**V**), and 4-chlorobenzylidenmalononitrile [2-(2-chlorophenyl)-1,1-dicyanoethylene] (**VII**) was performed using the Knoevenagel reaction from the corresponding F-, Cl-, or NO_2-substituted benzaldehydes and malononitrile [10–13]. Compounds were recrystallized from ethanol and showed no impurities by GC–MS before use.

2.2. X-ray analysis

Single crystals of **II, III** and **V** for X-ray analysis were grown by slow evaporation from ethanol solutions. Experimental data for crystals of **II** and **V** were obtained at low temperatures and for the crystal of **III** at room temperature with the four-circle diffractometers Syntex $P2_1$ (**II**, **III**) and Siemens P3/PC (**V**). The structures were solved by direct methods and refined by full-matrix least squares in anisotropic approximation for non-hydrogen atoms. The hydrogen atoms were localized on difference Fourier

Table 1
Crystal determination summary for compounds **II**, **III** and **V**

	II	**III**	**V**
Empirical formula	$C_{10}H_5FN_2$	$C_{10}H_5ClN_2$	$C_{10}H_5N_3O_2$
Formula weight	172.14	188.61	199.17
Temperature (K)	193(2)	298(2)	153(2)
Crystal size (mm)	0.2, 0.3, 0.3	0.3, 0.3, 0.4	0.2, 0.2, 0.3
Crystal system	Monoclinic	Monoclinic	Monoclinic
Space group	Pc	$P2_1/c$	$P2_1/n$
Z	2	4	4
Unit cell dimensions:			
a (Å)	3.8605(11)	3.9882(9)	7.443(2)
b (Å)	9.773(4)	21.139(5)	19.839(7)
c (Å)	11.029(4)	10.741(2)	7.023(2)
β (°)	95.39(3)	95.31(2)	118.121(14)
Volume Å^3	414.3(2)	901.7(4)	914.7(4)
Density (calc) (g cm^3)	1.380	1.389	1.446
Absorbtion coefficient (mm^{-1})	0.101	0.371	0.106
F (000)	176	384	408
Diffractometer used	Syntex $P2_1$	Syntex $P2_1$	Siemens P3/PC
θ range (°)	2.1–32.6	2.1–28.1	2.1–33.1
Scan range (ω, °)	1.80	1.80	1.80
Reflections collected	1704	2191	3521
Independent reflections	1700	1894	3309
Data/restraints/parameters	1645/0/138	1842/0/138	2817/0/156
Final R indices [$I > 2\sigma(I)$]	$R_1 = 0.058$	$R_1 = 0.034$	$R_1 = 0.051$
	$wR_2 = 0.112$	$wR_2 = 0.083$	$wR_2 = 0.115$
R indices (all data)	$R_1 = 0.129$	$R_1 = 0.053$	$R_1 = 0.113$
	$wR_2 = 0.146$	$wR_2 = 0.120$	$wR_2 = 0.175$
Largest difference peak (e/Å^3)	0.149	0.149	0.273
Largest difference hole (e/Å^3)	− 0.178	− 0.178	− 0.282

maps and refined isotropically. All calculations were performed with an IBM PC/AT-586 personal computer using the programs SHELXTL PLUS and SHELXL-93. Details of the data collection and structure refinement are given in Table 1. Atomic coordinates and their isotropic equivalent displacement parameters are given in Table 2, bond lengths, bond angles, and torsion angles are presented in Table 3. The general view of the molecules studied with atomic numbering schemes is presented in Fig. 1.

2.3. Database search

A search for monosubstituted derivatives of dicyanovinylbenzene has been performed with the LINUX version of the Cambridge Structural Database [14], October 1997 release. During this search one additional acentric compound, namely 4-chlorobenzylidenmalononitrile (**VII**) [15] was found, and its molecular and crystal structure and NLO properties are discussed in the present paper together with other compounds of this series.

2.4. Molecular mechanics and quantum chemical calculations

Molecular geometry for the compounds of interest was calculated using a quantum chemical approximation (GAUSSIAN 94 [16], RHF/6-31G** basis set) and molecular mechanics (MM3 [17,18]). The results of quantum calculations and X-ray analysis were used for the calculations of molecular hyperpolarizabilities.

For the computation of polarizabilities a modification of the static field method [19,20] developed in Refs. [21,22] was used. Multiple static-field calculations were performed using the MOPAC program [23] and the AM1 Hamiltonian. The polarization versus

Table 2
Atomic coordinates ($\times 10^4$) and equivalent isotropic displacement parameters ($Å^2 \times 10^3$) for compounds **II**, **III** and **V**. *U*(eq) is defined as one third of the trace of the orthogonolized U_{ij} tensor

Atom	*x*	*y*	*z*	*U*(eq)
Compound ***II***				
F(1)	7460(5)	1471(2)	2659(1)	47(1)
N(1)	9541(8)	7064(3)	1820(3)	47(1)
N(2)	2812(7)	5714(3)	−1291(2)	43(1)
C(1)	5241(6)	2449(2)	777(2)	25(1)
C(2)	5710(7)	1306(2)	1537(2)	30(1)
C(3)	4543(8)	16(3)	1211(3)	36(1)
C(4)	2738(8)	−168(3)	74(3)	37(1)
C(5)	2187(8)	942(3)	−724(3)	34(1)
C(6)	3403(7)	2233(3)	−377(2)	31(1)
C(7)	6679(6)	3751(2)	1226(2)	26(1)
C(8)	6381(7)	5012(2)	713(2)	28(1)
C(9)	8127(7)	6157(3)	1340(2)	33(1)
C(10)	4398(7)	5378(3)	−408(2)	31(1)
H(3)	5116(112)	−632(45)	1645(34)	53(11)
H(4)	2172(97)	−1087(40)	−191(34)	45(9)
H(5)	939(118)	793(45)	−1479(41)	67(13)
H(6)	2994(81)	2905(33)	−937(27)	27(7)
H(7)	7854(67)	3729(23)	1957(23)	12(6)
Compound ***III***				
Cl(1)	1278(1)	5914(1)	161(1)	59(1)
N(1)	−2(5)	8501(1)	1701(2)	81(1)
N(2)	6503(4)	7720(1)	4731(1)	65(1)
C(1)	3664(3)	6316(1)	2498(1)	39(1)
C(2)	3287(4)	5808(1)	1650(1)	43(1)
C(3)	4520(4)	5212(1)	1963(2)	57(1)
C(4)	6164(5)	5106(1)	3128(2)	62(1)
C(5)	6560(4)	5592(1)	3989(2)	58(1)
C(6)	5315(4)	6184(1)	3680(1)	50(1)
C(7)	2319(4)	6931(1)	2122(1)	40(1)
C(8)	2793(4)	7498(1)	2688(1)	40(1)
C(9)	1234(4)	8055(1)	2129(1)	52(1)
C(10)	4864(4)	7614(1)	3830(1)	45(1)
H(3)	4126(50)	4873(10)	1329(20)	78(6)
H(4)	6958(54)	4711(11)	3285(20)	81(6)
H(5)	7684(55)	5515(10)	4826(20)	75(6)
H(6)	5632(50)	6513(11)	4322(19)	73(6)
H(7)	954(40)	6948(7)	1342(16)	48(4)
Compound ***V***				
O(1)	6721(2)	4491(1)	1810(2)	35(1)
O(2)	8659(2)	3742(1)	1474(2)	48(1)
N(1)	1066(2)	5632(1)	2775(2)	45(1)
N(2)	3858(2)	3904(1)	7032(2)	39(1)
N(3)	7176(2)	3903(1)	1698(2)	27(1)
C(1)	4194(2)	3528(1)	2109(2)	21(1)
C(2)	5902(2)	3363(1)	1854(2)	22(1)
C(3)	6493(2)	2703(1)	1824(2)	26(1)
C(4)	5375(2)	2182(1)	2081(2)	28(1)
C(5)	3712(2)	2328(1)	2397(2)	27(1)
C(6)	3127(2)	2992(1)	2407(2)	24(1)
C(7)	3379(2)	4216(1)	1920(2)	22(1)
C(8)	2901(2)	4483(1)	3384(2)	23(1)
C(9)	1878(2)	5125(1)	3032(2)	29(1)
C(10)	3408(2)	4157(1)	5407(2)	26(1)
H(3)	7693(29)	2628(9)	1591(29)	41(5)
H(4)	5759(25)	1718(9)	2103(26)	31(4)
H(5)	2910(25)	1978(8)	2547(27)	30(4)
H(6)	1932(27)	3096(9)	2615(27)	33(4)
H(7)	3115(25)	4454(8)	701(27)	28(4)

static field data was then processed into polynomial expansions of variable degrees using the HYPER program [22], according to Eq. (1).

$$P_q = \mu_q + \sum_j \alpha_{qj}F_j + \sum_j \sum_k \beta_{qjk}F_jF_k + \sum_j \sum_k \sum_l \gamma_{qjkl}F_jF_kF_l + \cdots \quad (1)$$

where P_q represents the qth component of the polarization, F_i the ith component of the applied electric field, μ the permanent dipole moment, α the linear polarizability, β and γ the second- and third-order polarizabilities, respectively. In this program, the necessary tensor elements and their associated numerical uncertainties are used to construct the values of the non-linear properties, according to Eqs. (2)–(4):

$$\beta_q = \beta_{qqq} + (1/3)[\sum_{j\neq k}(\beta_{qjj} + \beta_{jqj} + \beta_{jjq})] \quad (2)$$

$$\beta_{vec} = (\sum_q \beta_q^2)^{1/2} \quad (3)$$

$$\gamma = (1/5)\{\sum_j [\gamma_{jjjj} + (1/2)\sum_{k\neq j}(\gamma_{jjkk} + \gamma_{kkjj})]\}. \quad (4)$$

2.5. Modeling of crystal morphology

The theoretical basis and method for crystal habit calculations was previously described [24,25]. The program package NONVPOT [26], modified by us, was used for crystal shape calculations based on experimental data of the molecular crystal structure. The atom–atom potential method was used to calculate intermolecular energy, energy of molecular

Table 3
Bond lengths (Å), bond angles, and torsion angles (°) in structures **II**, **III** and **V**

	II	**III**	**V**
F(1)–C(2)	1.363(3)		
Cl(1)–C(2)		1.736(2)	
N(3)–C(2)			1.468(2)
O(1)–N(3)			1.227(2)
O(2)–N(3)			1.228(2)
N(1)–C(9)	1.144(4)	1.141(2)	1.144(2)
N(2)–C(10)	1.149(3)	1.139(2)	1.143(2)
C(1)–C(2)	1.398(3)	1.407(2)	1.404(2)
C(1)–C(6)	1.413(3)	1.403(2)	1.401(2)
C(1)–C(7)	1.456(3)	1.450(2)	1.473(2)
C(2)–C(3)	1.375(4)	1.382(2)	1.385(2)
C(3)–C(4)	1.389(4)	1.376(3)	1.391(2)
C(4)–C(5)	1.400(4)	1.381(3)	1.387(2)
C(5)–C(6)	1.387(4)	1.377(2)	1.389(2)
C(7)–C(8)	1.356(3)	1.349(2)	1.345(2)
C(8)–C(10)	1.437(3)	1.435(2)	1.439(2)
C(8)–C(9)	1.448(3)	1.437(2)	1.444(2)
C(2)–C(1)–C(6)	116.5(2)	116.61(13)	116.97(11)
C(2)–C(1)–C(7)	118.1(2)	119.29(12)	124.29(11)
C(6)–C(1)–C(7)	125.4(2)	124.09(12)	118.57(11)
F(1)–C(2)–C(3)	117.9(2)		
F(1)–C(2)–C(1)	118.4(2)		
C(3)–C(2)–Cl(1)		117.75(11)	
C(1)–C(2)–Cl(1)		120.70(11)	
C(1)–C(2)–N(3)			119.72(11)
C(3)–C(2)–N(3)			117.87(11)
O(1)–N(3)–C(2)			118.68(10)
O(2)–N(3)–C(2)			118.10(11)
O(2)–N(3)–O(2)			123.22(11)
C(3)–C(2)–C(1)	123.7(2)	121.54(14)	122.37(11)
C(2)–C(3)–C(4)	118.7(2)	119.9(2)	119.16(12)
C(3)–C(4)–C(5)	120.0(3)	120.2(2)	119.96(12)
C(6)–C(5)–C(4)	120.3(2)	119.9(2)	120.25(12)
C(5)–C(6)–C(1)	120.8(2)	121.8(2)	121.25(12)
C(8)–C(7)–C(1)	129.6(2)	129.64(12)	122.81(11)
C(7)–C(8)–C(10)	127.0(2)	125.66(12)	122.48(11)
C(7)–C(8)–C(9)	119.1(2)	120.14(12)	121.65(11)
C(10)–C(8)–C(9)	113.9(2)	114.18(12)	115.85(11)
N(1)–C(9)–C(8)	178.9(3)	179.0(2)	179.2(2)
N(2)–C(10)–C(8)	177.8(3)	178.4(2)	178.36(14)
C(2)C(1)C(7)C(8)	− 174.9(2)	169.1(1)	− 132.1(2)
C(1)C(7)C(8)C(9)	− 179.0(2)	178.9(1)	− 172.4(2)
C(1)C(7)C(8)C(10)	2.7(2)	0.8(1)	8.9(2)
C(6)C(1)C(7)C(8)	5.4(2)	11.8(1)	52.7(2)
O(1)N(3)C(2)C(1)			0.5(2)
O(2)N(3)C(2)C(1)			0.0(2)
O(1)N(3)C(2)C(3)			− 177.0(2)
O(2)N(3)C(2)C(3)			2.5(2)

layers, attachment energy, and relative rates of crystal face growth. The "theoretical form" of the crystal was defined as the polyhedron delimited by the most stable faces. From our calculations we could obtain the vectors normal to crystal faces and the relative rates of crystal face growth, thus, we could build theoretical crystal shapes based on geometric considerations.

We calculated the intermolecular energy using Williams' parameter [27] for "6-exp" energy functions. The final result of the calculations was the coordinates of the polyhedron vertexes. The SHELXTL program was used for the graphical presentation of crystal shapes.

2.6. Evaluation of second harmonic efficiency and second-order microscopic non-linearity

We investigated experimental second harmonic efficiency and second-order microscopic non-linearity for compounds **II**, **III** and **VII.** In accord with results of the X-ray study two of them (namely **II** and **VII**) belong to the acentric space groups (Table 1), and according to quantum chemical calculations all these compounds should display second order non-linearity in solution.

The schematic diagram of the experimental setup is presented in Fig. 2. Powder experiments were performed using the Kurtz technique at the wavelength of 1064 nm. A Q-switched Nd:YAG laser with near Gaussian optics and 10 ns pulses was used as a primary source. The laser beam was split into two using a partially reflective mirror. The weaker reflected beam was used to generate second harmonic (SH) light from a quartz crystal and the other part was focused on the powder samples placed on the thin glass slides. The samples were mounted at the focal point of a parabolic mirror and the scattered SH light was collected and converged toward a photomultiplier tube (Hamamatsu R268UH) using a lens system. The signal from the quartz crystal was used as a reference to make corrections for fluctuations in the laser power. The SH signals were detected after filtering them to remove remaining fundamental light and any spurious signals by using broad band and interference filters. Neutral density filters were also used to attenuate the signal in order to avoid any detector saturation.

The second-order microscopic non-linearities of compounds **II**, **III**, and **VII** in solutions were

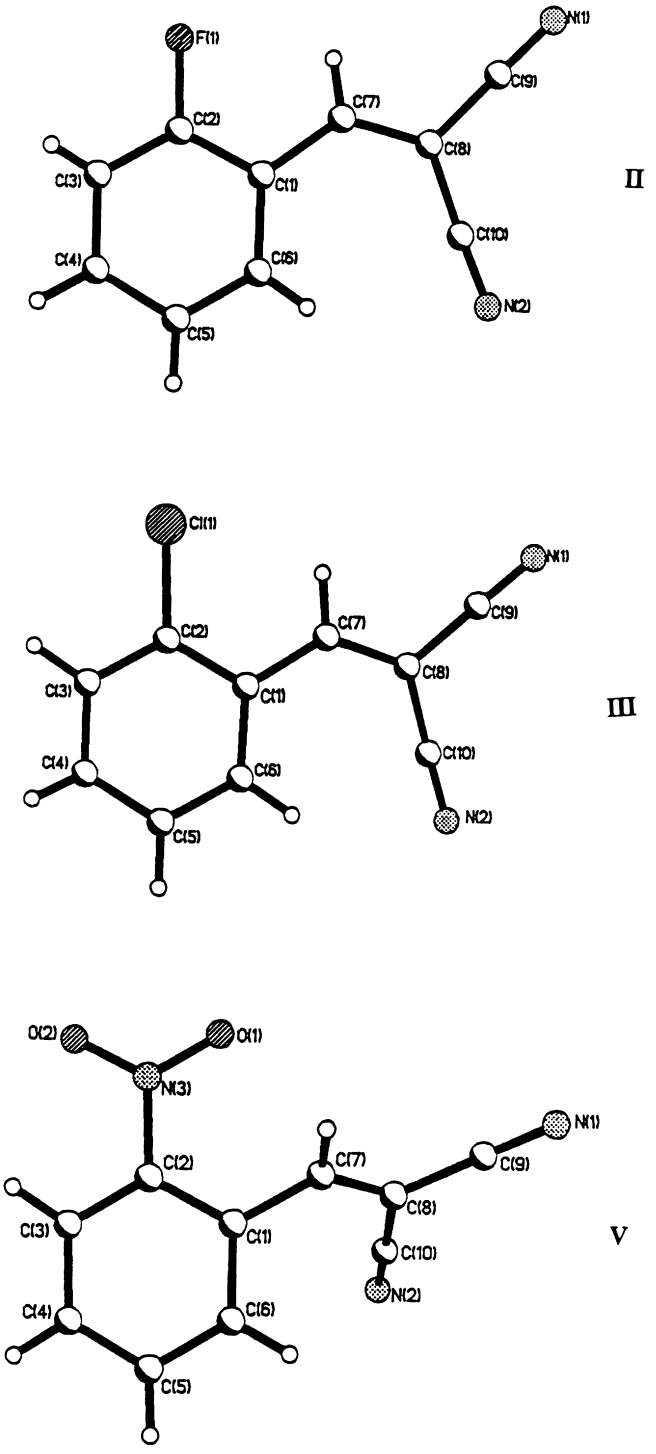

Fig. 1. General view of molecules **II**, **III** and **V** with atomic numbering schemes.

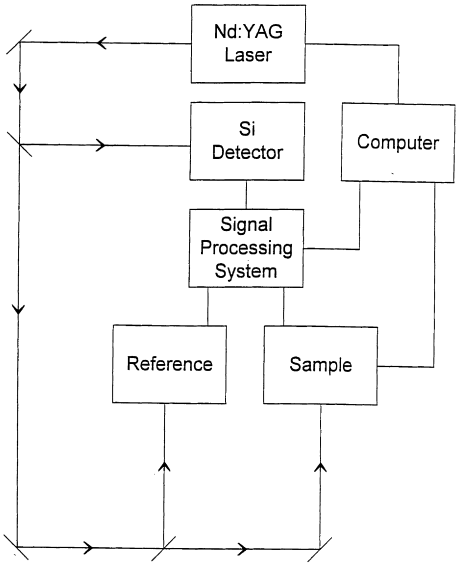

Fig. 2. The basic configuration setup for both powder and EFISH experiments.

investigated using the electric field induced second harmonic generation (EFISH) technique [5,28–30]. All measurements were taken in chloroform solution because of the low solubility of the compounds studied in 1,4-dioxane. The same laser used in the powder experiments was utilized in the EFISH setup as the primary source and it was operated at a pulse repetition rate of 10 Hz. An adequately clean beam with sufficient energy (about 5–10 mJ) was obtained by using a high power spatial filter. A set of polarizing elements was used to control the intensity and the state of polarization of the beam. The SH signal was measured as a function of the intensity of the fundamental beam and the angle of incidence for each material.

In our EFISH experimental setup many sources of error associated with the conventional EFISH technique have been eliminated. The configuration of our EFISH setup was somewhat similar to the modified EFISH method introduced first by Uemiya et al. [31] in 1993, and which was independently developed by us during the same period [32]. One of the major differences between this method and the conventional EFISH technique was the use of a liquid cell with a unique geometry. It consisted of two indium tin oxide (ITO) coated, transparent, glass windows, with dimensions $60 \times 30 \times 1\ mm^3$ and a 1–3 mm thick flat glass spacer with a 12 mm diameter hole. The ITO coated conductive glasses served as both windows and high voltage electrodes. The spacer was sandwiched between the windows, and the resulting disk shaped cavity defined the volume of the liquid sample. The conductive layer of each window was on the internal surface; hence, the DC electric field, E_0, existed only in the liquid and across the spacer. The cell was mounted at the center of a computer controlled positioning system consisting of a rotational stage with a vertical axis of rotation and two translational stages with motion in horizontal and vertical directions. The experimental configuration is described in detail elsewhere [33].

The EFISH intensity generated by a solution with dipolar solute molecules is given by

$$2, \omega, Z = C_Z(n_\omega, n_{2\omega})[\chi^{(3)}_{ZZZZ}(-2\omega; \omega, \omega, 0)]^2 E_0^2 I^2_{w,Z,} \tag{5}$$

where

$$[\chi^{(3)}_{ZZZZ}(-2\omega; \omega, \omega, 0)]^2 = F\left(\frac{\partial I_{2\omega,Z}}{\partial c}, \frac{\partial f_\omega}{\partial c}, \frac{\partial f_{2\omega}}{\partial c}, \frac{\partial f_0}{\partial c}\right) f_\omega^4 f_{2\omega}^2 f_0^2 \left[N_u^2 \left(\gamma_{z,u} + \frac{\beta_{z,u}\mu_{z,u}}{5kT} \right)^2 + N_u^2 \left(\gamma_{z',v} + \frac{\beta_{z',v}\mu_{z',v}}{5kT} \right)^2 \right] \tag{6}$$

In Eqs. (5) and (6), N is the number density, c the concentration of the solution, $I_{\omega,Z}$ the intensity of the fundamental beam with the state of polarization Z; f_ω, $f_{2\omega}$ and f_0 are the local field correction factors at the frequencies ω, 2ω and 0, respectively, γ the scalar part of $\gamma(-2\omega; \omega, \omega, 0)$, β_z the component of the vector of $\beta(-2\omega; \omega, \omega)$ along the direction of the ground-state dipole moment μ_z.

The factor C_Z depends on the geometry of the medium and optical transmission through the medium, as well as on the direction of polarization that needs to be non-perpendicular to the applied static field E_0. The subscripts u and v refer to the solute (compounds **II**, **III** or **VII**) and solvent (chloroform), respectively, and the correction factor F represents the solute–solute interactions which can be taken into account using an infinite dilution technique [28].

According to Eq. (5), in order to generate SH, the

Table 4
Experimental X-ray values of torsion angles C(6)C(1)C(7)C(8), ° (τ) in crystals **I**–**XII**

Molecule	τ	Reference	Molecule	τ	Reference
I	−9.9	[5]	**VII**	−0.8	[15]
II	5.4	Present work	**VIII**	−2.8	[5]
III	11.8	Present work	**IX**	−6.4	[7]
IV	−9.9	[5]	**X**	−1.1	Unpublished results
V	52.7	Present work	**XI**	13.7	[38]
VI	21.9	[36]	**XII**	−13.8	[37]

static and dynamic electric fields must be parallel and, therefore, a non-zero angle of incidence is necessary. This specific geometry of the cell caused $C_Z(n_\omega, n_{2\omega})$ to oscillate as the angle of incidence is varied [34]. Therefore, a maker interference pattern was obtained by rotating the cell from about 45–50°.

The samples were gradually diluted and the SH intensity was measured as a function of concentration. The range of concentrations varied from 0.01 to 0.12 M. The average maximum of the fringes was used to estimate the induced SH intensity, and hence, $\chi^{(3)}_{ZZZZ}$ as determined using a known material (*para*-nitroaniline in chloroform) as the reference. The microscopic second-order susceptibility of each compound was determined by using appropriate local field correction factors.

A value of $(20.5 \pm 0.8) \times 10^{-30}$ esu has been obtained for the β of *para*-nitroaniline using quartz as a reference. The d_{11} value used for quartz in our analysis was 1.13×10^{-9} esu. In an earlier work with EFISH measurements [29], a magnitude of 0.80×10^{-9} esu has been used for the same d_{11} value. However, based on the study published by Choy and Byer [35], the value of 1.13×10^{-9} esu has been considered as the standard, and therefore, in our work all β values determined were based on that reference value. The β values obtained for compounds **II**, **III** and **VII** were found to be 9.8×10^{-30}, 9.2×10^{-30} and 12.5×10^{-30} esu, respectively. The uncertainty of the final results was less than 5%.

3. Results and discussion

3.1. Molecular geometry

The molecular geometry of the molecules studied (Fig. 1, Table 3) is not unexpected for this class of compounds. Molecules **II** and **III** form different crystal structures but have nearly identical geometry parameters. The only noticeable difference is the torsion angle between the aromatic ring and the dicyanovinyl group (5.4 and 11.8°, respectively, see Table 4), and the bond angles at the C(1) and C(2) atoms of the ring (Table 3). In particular, the *ipso*-angles C(1)C(2)C(3) reflect different acceptor ability of substituents, while different exocyclic angles may be the result of steric demands of *o*-substituents. Most geometry parameters of molecule **V** are close to those for **II** and **III**, however the above mentioned torsion angle is significantly larger (52.7°) in **V** because of steric hindrance between the neighboring nitro- and dicyanovinyl groups.

Only a few *o*- and *p*-substituted derivatives of benzylidenmalononitrile were found in CSD. Several other derivatives of this series have been investigated and the corresponding results are published in Refs. [5,7,10]. Most molecules of interest in crystals are characterized by a planar or almost planar conformation reflecting a π-conjugation between the benzene ring and the dicyanovinyl residue. For most compounds, the torsion angle C(Ph)–C(Ph)–CH=C(CN)$_2$ characterizing a molecular non-planarity is less than 15° (Table 4). This angle is larger only for molecules **V** and **VI** having bulky substituents in the *ortho*-position of the ring. Remarkably, for these molecules, small deviations from the planar conformation are not always related to intramolecular steric interactions. For instance, such interactions should be small for molecule **I** (no non-hydrogen substituents in the *o*- and in the *p*-position) and molecules **XI** and **XII** (substituents only in *p*-positions). However, for all these molecules a noticeable non-planarity in the crystal state has been observed (Table 4). These

Table 5
Comparison of the experimental results and the results of MM and ab initio geometry calculations for molecules **I–V** and **VII**

Molecule	C(6)C(1)C(7)	C(1)C(7)C(8)	C(2)–C(1)–C(7)	C(6)C(1)C(7)C(8)	X–C(2)–C(1)–C(7)[a]	Total energy (a.u.)
I						
X-ray	124.8	130.9	116.7	− 9.9	− 3.2	
MM	124.7	129.8	117.8	0.0	0.0	
Ab initio	125.1	132.1	116.3	0.0	0.0	− 491.0574691
II						
X-ray	125.4	129.6	118.1	5.4	0.5	
MM	124.2	129.1	118.5	0.0	0.0	
Ab initio[b]	126.0	131.3	117.2	0.0	0.0	− 589.9057841
Ab initio	125.8	131.0	117.3	10.3	0.5	− 589.9057879
III						
X-ray	124.1	129.6	119.3	11.8	0.7	
MM	123.2	129.2	120.1	0.0	0.0	
Ab initio[b]	123.3	131.6	119.6	0.0	0.0	− 949.9486888
Ab initio	121.7	127.8	120.4	38.6	2.6	− 949.9501858
IV						
X-ray	125.0	129.6	116.5	− 9.9	0.9	
MM	123.5	130.1	118.6	0.2	0.4	
Ab initio[b]	124.5	131.9	117.2	0.0	0.0	− 604.9422038
Ab initio	123.8	130.1	117.6	− 24.3	− 1.8	− 604.9424346
V						
X-ray	118.5	122.8	124.3	52.7	9.3	
MM	120.4	124.5	121.8	48.1	3.9	
Ab initio	118.9	125.3	123.9	51.4	4.4	− 694.5148251
VII						
X-ray	123.7	130.7	116.7	− 11.7	− 0.8	
MM	124.6	129.0	118.2	0.0	0.0	
Ab initio	152.2	132.0	116.4	0.0	0.0	− 949.9536048

[a] X—key-atom of the substituent in *ortho*-position.
[b] Local minimum for planar conformation.

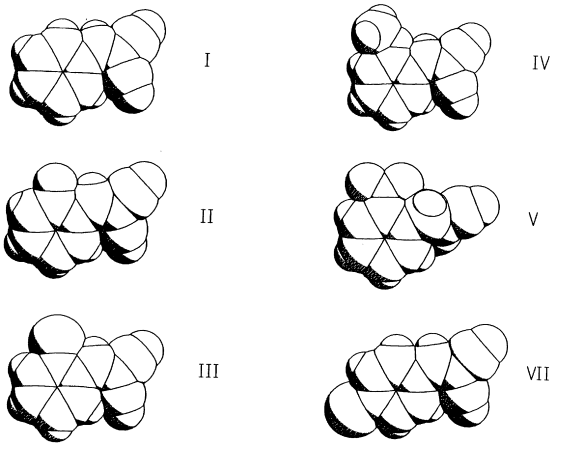

Fig. 3. Molecular shape of the molecules **I–V** and **VII**. For space-filling models the van der Waals radii of atoms C, H, N and O were used.

results may be related to the influence of the crystal packing on molecular geometry.

Different steric requirements of the substituents in the structures studied result in some other distinctions in their geometry. Several geometry parameters for molecules **I–V** and **VII** from the results of X-ray analysis, quantum chemical and molecular mechanics calculations are compared in Table 5. Some features of these molecules should be mentioned. The C(1)C(7)C(8) and C(6)C(1)C(7) bond angles in structure **V** are the smallest when compared with molecules **I-IV** and **VII**, and the C(2)C(1)C(7) angle in molecule **V** is the largest. These results are also understandable in terms of steric requirements for the substituents and requirements of planarity of these molecules because of the π-conjugation between the benzene ring and the dicyanovinyl fragment (molecules **I–VII**) and between the benzene ring and the

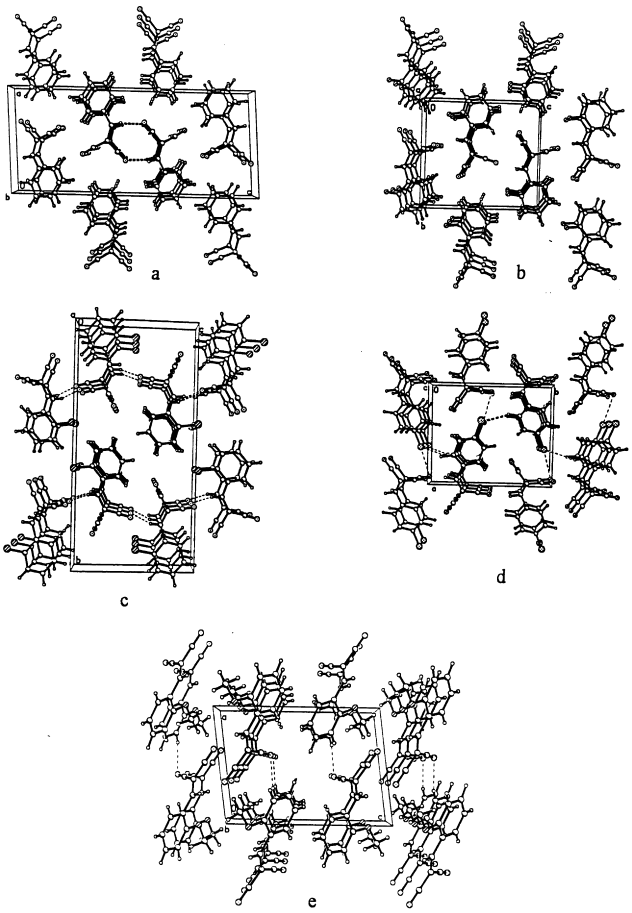

Fig. 4. Molecular packing diagrams for compounds **I**–**IV** and **VII**: (a) structure **I**, projection along the crystal *b*-axis; (b) structure **II**, projection along the *a*-axis; (c) structure **III**, projection along the *a*-axis; (d) structure **VII**; projection along the *c*-axis; (e) structure **IV**, projection along the *b*-axis.

NO_2-group (molecule **V**). A planar geometry for molecules **I**–**IV** and **VII** (see atom numbers in Fig. 1) leads to two short intramolecular contacts between the CN-group (atoms C(10) and N(2)) and a hydrogen at atom C(6) on one side of the dicyanovinyl fragment, and to one short contact between a hydrogen atom at C(7) and a substituent at the *ortho*-position on the other side of this fragment. Most likely these two short contacts in molecules **I**–**IV** and **VII** are reflected by the enlargement of the C(1)C(7)C(8) and the C(6)C(1)C(7) bond angles. As short contacts are presented on both sides of the dicyanovinyl group in molecule **V** (with the nitro-group in the *ortho*-position coplanar to the benzene ring), the dicyanovinyl group has a skewed geometry not coplanar with the benzene ring (Table 5). The different steric requirements of the substituents are visible in Fig. 3, demonstrating the van der Waals shapes of molecules **I**–**V** and **VII**. The above explanation in terms of steric requirements was validated by the fact that MM calculations, which reflect steric intramolecular interactions, were close to the experimental results (Table 5).

On the contrary, and to our surprise, crystal conformation of the molecules of this series was not reproduced with accuracy by quantum chemical calculations. We optimized the geometry of molecules **I**–**V** and **VII** using the RHF/6-31G** approximation, from two starting geomertries without any geometry restrictions. The first starting geometry was chosen in agreement with the results from the

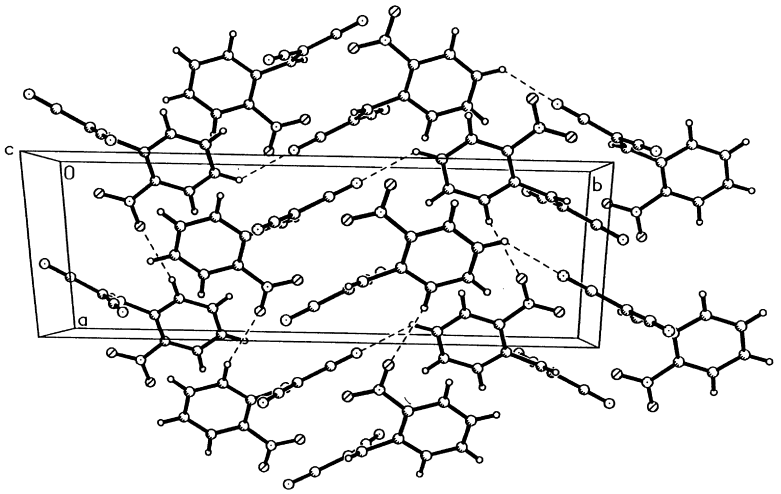

Fig. 5. Molecular packing diagram for compound **V**, projection along the crystal *c*-axis.

Table 6
Atomic charges (e) in molecules **I**–**V**and **VII** according to ab initio (6-31G**) calculations.Atom numbers indicyanovinylbenzene fragment correspond to Fig. 5, numbers of key atoms in substituents (OMe, Hal) and H atoms correspond to their positions, atoms in nitro-group (molecule**V**) denoted as N(3), O(3), and O(3′)

Atom	**I**	**II**	**III**	**IV**	**V**	**VII**
C(1)	− 0.042	− 0.145	− 0.004	− 0.144	− 0.043	− 0.046
C(2)	− 0.138	0.466	− 0.172	0.463	0.157	− 0.132
C(3)	− 0.157	− 0.215	− 0.120	− 0.225	− 0.102	− 0.122
C(4)	− 0.126	− 0.118	− 0.121	− 0.111	− 0.156	− 0.149
C(5)	− 0.161	− 0.172	− 0.162	− v.184	− 0.121	− 0.126
C(6)	− 0.131	− 0.115	− 0.125	− 0.111	− 0.133	− 0.124
C(7)	− 0.016	− 0.008	− 0.028	0.012	0.038	− 0.016
C(8)	− 0.037	− 0.029	− 0.027	− 0.044	− 0.016	− 0.032
C(9)	0.298	0.299	0.298	0.297	0.309	0.298
C(10)	0.319	0.318	0.320	0.318	0.301	0.318
N(1)	− 0.437	− 0.435	− 0.433	− 0.445	− 0.426	− 0.433
N(2)	− 0.456	− 0.455	− 0.453	− 0.464	− 0.432	− 0.453
H(2)	0.169					0.179
H(3)	0.168	0.189	0.191	0.168	0.233	0.193
H(4)	0.170	0.180	0.179	0.171	0.187	
H(5)	0.172	0.177	0.180	0.170	0.189	0.197
H(6)	0.204	0.211	0.209	0.206	0.197	0.213
H(7)	0.201	0.228	0.228	0.234	0.233	0.204
F(2)		− 0.376				
Cl(2)			0.040			
O(2′)				− 0.682		
C(Me)				− 0.037		
H(Me1)				0.154		
H(Me2)				0.127		
H(Me3)				0.127		
N(3)					0.514	
O(3)					− 0.478	
O(3′)					− 0.451	
Cl(4)						0.031

MM structure optimization (planar geometry for all molecules except **V**). For the second starting geometry, we increased the torsion angle between the benzene ring and the dicyanovinyl fragment from 0 to 10°. We obtained optimized geometries for two local minima for molecules **II**–**IV** and one minimum for molecules **I**, **V** and **VII**. Some of the results on the geometry of these molecules are listed in Table 5. In our calculations, the non-planarity of molecules **II**–**IV** was more pronounced than from X-ray data in the crystal. Again, intermolecular interactions in the crystals could explain the geometry, as the energy difference between the planar and non-planar conformations were extremely small (0.002, 0.939 and 0.145 kcal mol^{-1} for **II**, **III** and **IV**, respectively).

3.2. Molecular crystal packing

A molecular packing diagrams for compounds **II** and **III** are represented in Fig. 4 and for compound **V** in Fig. 5. Packing diagrams for compounds **I**, **IV** and **VII**, which were studied earlier, are also represented in Fig. 4 for comparison. No short intermolecular contacts were found in structure **II**. In structure **III**, one short intermolecular contact was found [H(7)···N(2), 2.46(3) Å] with molecule 1 + X, 1.5 − Y, 0.5 + Z forming molecular chains along the *c*-axis (Fig. 4). The crystal unit cell for compound **III** was approximately twice as large as for compound **II**, and centrosymmetric when compound **II** crystallize in an acentric space group. The packing mode of the non-planar compound **V** differed from that of **II** and **III** (Fig. 5). Two short intermolecular contacts were found in this structure [N(1)···H(4), 2.562 Å,with molecule 0.5 − X, 0.5 + Y, 0.5 − Z and O(2)···H(6) 2.515 Å, with molecules X, Y, 1 + Z].

It is not surprising that the molecular packing patterns for several compounds from this series (**I**–**IV** and **VII**) resembled each other (Fig. 4). It is probably because of the similar shapes of these molecules (Fig. 3). In spite of their similar crystal packing modes, these compounds are described by several different space groups (**I** $P2_1/c$, **II** Pc, **III** $P2_1/c$, **IV** $P2_1$, **VII** $P2_1$). We tried to understand the influence of both steric and electrostatic interactions, on a qualitative level, using data on their molecular van der Waals shapes and charge distributions from our ab initio calculations. The results of the quantum chemical calculations of the net charge distributions in molecules **I**–**V** and **VII** are presented in Table 6.

In structure **I**, molecules are joined in centrosymmetric dimers with short intermolecular contacts N(2)···H(7) 2.568 Å, 2 − X, −1 − Y, −Z (Fig. 4(a)). In structure **IV**, chains parallel to $a + b$ are formed with a short intermolecular contact N(1)···H(3) 2.495 Å, −1 + X, −1 + Y, Z (Fig. 4(e)). In structure **VII** (Fig. 4(d)), two short contacts should be mentioned: Cl(1)···H(6) 2.875 Å −1 − X, 0.5 + Y, −Z, and Cl(1)···N(13) 3.283 Å 1 + X, Y, −1 + Z. One can see that, in most of the short intramolecular contacts found, the nitrogen atoms from the cyano-groups are involved (structures **I**, **III**, **IV**, **V** and **VII**). This is understandable as nitrogen atoms of the cyano-groups in all molecules were characterized by noticeable negative charges (Table 5). Significant positive charges were located on the hydrogen atoms of the C=C bridges, and they were also often involved in the short intramolecular contacts (structures **I** and **III**). The other "charged" hydrogen atom H(6) was involved in the short intermolecular contact in structure **VII**. The character of the net charge distribution in molecules **II** and **III** differ significantly. The halogen atom in **II** was "charged", while in **III** its charge is negligible. Maybe the presence of several negatively charged atoms on the molecular "surface" of molecule **II** (atoms N(1), N(2), F(2)), together with positive charged atoms (C(2), C(9), C(10)) on the "background", led to the absence of short intermolecular contacts in this structure. It is obvious that all packing patterns found for the investigated compounds were determined by a gentle balance between van der Waals (steric) and electrostatic requirements in the crystals; in several cases, leading to an acentric molecular packing and, in other cases, to a centrosymmetric type. Of course, these explanations are quite qualitative but future energy calculations in crystals may reveal, in greater detail, the reasons why a particular crystal packing is preferred.

3.3. Evaluation of NLO properties

In the powder experiments, the acentric compounds **II** and **VII** generated a very strong visible green (532 nm) SH light when they were illuminated by the fundamental beam pulses with moderate energy. The SH signal generated by compound **III** under the

Table 7
Calculated dipole moments (μ, D) and second-order polarizabilities (β, 10^{-51}C m^3 V^{-2}) for molecules **I–V** and **VII**

Molecule[a]		μ	β	γ	Exptl β	Reference
I	pl	4.578	12.632	3.390	22.75	[5]
	X-ray	4.646	12.889	3.505		
II	pl	4.595	10.175	3.424	34.16	
	npl	4.576	9.982	3.373		
	X-ray	4.320	10.030	3.625		
III	pl	4.414	9.796	3.514	36.38	
	npl	4.232	6.641	2.664		
	X-ray	4.151	9.915	3.588		
IV	pl	6.312	14.541	4.047	18.71	[5]
	npl	6.122	12.870	3.746		
	X-ray	6.451	14.875	4.168		
V	npl	5.808	0.672	1.962		
	X-ray	5.856	1.382	2.104		
VII	pl	3.365	20.457	5.002	46.40	
	X-ray	3.242	18.706	4.492		

[a] Computational results for α, β and γ corresponds to planar geometry obtained from ab initio calculations (pl), non-planar ab initio geometry (npl), and X-ray geometry (X-ray).

same conditions was barely visible. In order to compare the efficiency of the SH generation of each compound, urea samples in the form of powder with the particle size close to that of compounds **II**, **III** and **VII** were used as a reference.

At 1064 nm, the SH (532 nm) generation efficiencies for compounds **II** and **VII** was about 12–14 and 20–22 times greater than that of urea, respectively. The SH efficiency of compound **III** was much smaller than that of urea and the ratio was estimated to be about 0.4–0.5 within the experimental uncertainty. This is quite understandable, as X-ray analysis showed that compound **III** belonged to a centrosymmetric space group.

The β values, obtained from EFISH measurements for compounds **II**, **III** and **VII**, were 9.8×10^{-30}, 9.2×10^{-30} and 12.5×10^{-30}esu, respectively. Table 7 contains these results in SI units.

The calculated polarizability values for molecules **I–V** and **VII** are listed in Table 7. In addition to the β values obtained using optimized geometries from ab initio calculations, we have included polarizability calculations using local "planar" minima geometries, whenever the absolute minimum did not correspond to the planar structure.

It is important to mention that, as a result of the search for molecules (molecular modeling and database screening) with shape and packing mode suitable for SHG, two new compounds have been found. One of them (**II**) was synthesized and described in the present work, and the other (**VII**) was previously synthesized [13]; nevertheless, both compounds have been studied in the present work in terms of their potential for NLO.

Fig. 6 compares the β experimental values for compounds **I–IV** and **VII**, with the calculated values

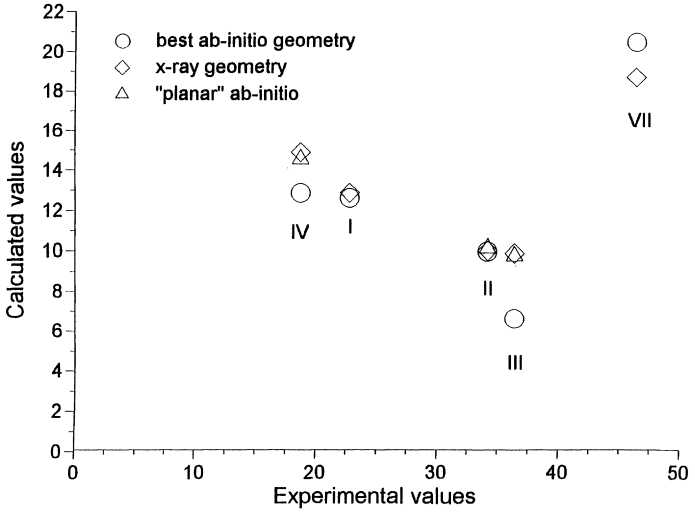

Fig. 6. Comparison between experimental and calculated second-order polarizability (β) values. Units: 10^{-51} Cm^3 V^{-2}.

obtained using X-ray geometries, as well as the geometries at the absolute minima and "planar" minima from ab initio calculations. The absolute minima for **I** (unsubstituted compound) and **VII** (*para*-Cl compound) in our ab initio calculations corresponded to planar structures. As shown in Table 5, the absolute energy minima for molecules **II**, **III** and **IV** (*ortho*-F, *ortho*-Cl, and *ortho*-methoxy compound, respectively) were found for conformations with the benzene ring twisted with respect to the vinyl group. The two geometries utilized for compound **I** and the three geometries utilized for compound **II** gave essentially the same calculated polarizabilities. The X-ray geometry and the "planar" geometry for compounds **III** and **IV** also gave essentially the same calculated polarizabilities, whereas their best ab initio geometries gave β values 32 and 11% lower, respectively.

Even though the "planar" conformation for compound **VII** corresponded to its absolute minimum, the geometry from X-ray data and this geometry gave calculated polarizability values differing by about 9%. In the X-ray geometry for **VII**, the vinyl group was slightly skewed with respect to the benzene ring (by about 12°, see Table 5). This torsion cannot explain the difference between the two β calculations for **VII**, as it is similar to the torsion angle difference between the X-ray and "planar" ab initio geometries for **III**. Thus, a charge-transfer effect might be invoked, which could be supported by the charge differences in atoms C(1), C(2) and C(5) (Table 6) between compounds **III** and **VII**; the *para*-Cl compound (**VII**) has lower electron density at C(2) and C(5) while higher electron density at C(1) than the *ortho*-Cl compound (**III**).

As the experimental β values for **II** and **III** are very close, there is some reason to believe that the solvent has an effect on the planarity of **III**, similar to the crystal (**II** was planar in the gas phase, while **III** was skewed). Thus, the planar ab initio geometry or the almost planar X-ray geometry for molecule **III** seems to represent better what occurs in solution.

Fig. 6 shows the polarizability values separated into three groups: the first group containing **I** and **IV**, the second group **II** and **III**, and **VII** in a group by itself. This is true for both the experimental values and the calculations. In that sense, the computations have reproduced the trends detected in the experimental β values. The grouping is related to both type of substituent and location, as the unsubstituted and *ortho*-methoxy (a weak electron donor) are in the first group, the two *ortho*-halogens (slightly electron withdrawing) in the second group, and the *para*-Cl stands by itself.

The difference in absolute values between the computational and experimental β values might be explained by the influence of the solvent ($CHCl_3$, $\varepsilon = 4.806$) and by dispersion effects due to the use of a dynamic field (1064 nm). In Ref. [5], a similar comparison between calculated and EFISH measurements on a series of methoxy derivatives of dicyanovinylbenzenes resulted in a linear relationship, with a correlation coefficient of 0.97 (from a least-squares regression), corresponding to a line passing through the origin and a slope of about 0.5. The value of the slope provided a correction factor for the calculated values of 2, which could account for solvent (in this case 1,4-dioxane) and dispersion effects (also at 1064 nm) on this type of molecules. Similarly, in Ref. [30], a comparison between calculated and experimental values on a series of Schiff's bases resulted in a correction factor of 3 (from a least-squares line passing through the origin and having a correlation coefficient of 0.91). In the present case, the dissimilarity on the nature of the substituents has been clearly shown. The correction factor for the calculated values (to account for the experimental conditions) for the first group would be in the vicinity of 1.5; for the *ortho*-halogens around 3.5; and close to 2 for the *para*-Cl compound.

As it was expected, our calculations showed that the molecule with two-acceptor substituents (**V**) was characterized by a very low β value. The largest β value in the series studied was found for the acentric compound **VII** with acceptor substituent in *para*-position. This compound is a good candidate molecule for further investigation of its NLO properties.

3.4. Crystal morphology

On the basis of X-ray data obtained in the present work and our previous investigation [5], we calculated the crystal morphology for potential NLO materials (compounds **II**, **IV** and **VII**), that crystallize in acentric space groups. The morphology of compound **IV** was described before [39], and compound **II** was

Table 8
Calculated crystal faces (for acentric crystals **II, IV** and **VII**), energy of the molecular layers parallel to these faces and relative faces areas

Face index	Layer energy	Face area
Crystal **II**		
010	−24.52	8.11
0–10	−24.51	8.11
011	−23.32	4.43
0–11	−23.32	4.43
001	−20.84	2.47
00–1	−20.84	8.17
100	−10.49	3.05
−100	−10.49	2.50
101	−11.88	1.87
−10 to 1	−11.88	2.47
Crystal **IV**		
100	−22.90	4.07
10–1	−21.56	2.61
010	−20.60	4.74
001	−18.60	3.16
Crystal **VII**		
100	−27.05	4.55
010	−25.69	4.56
001	−10.55	2.79
011	−9.13	0.57
1–10	−25.66	3.31
110	−25.62	3.26
−101	−8.96	0.59

studied in the present work. Experimental investigations of the properties of these compounds (EFISH and morphology investigations) were complicated by the fact that one of the compounds studied (**III**) is a very well-known lacrymator [40] and the halogen derivatives of the members of the series under study appear to have the same property, although to a different extent.

The initial molecular coordinates for the energy calculations were taken from the results of X-ray analysis. Some results of energy calculations (energy of the intermolecular interactions in crystal layers parallel to the developed crystal faces) and relative area of the faces are shown in Table 8.

The crystal shapes in two orientations (crystals **II**, **IV** and **VII**), and the face indexes are shown in Fig. 6. The crystal shapes have been drawn with the SHELX program. The calculated angles between the faces found for the "theoretical" shape in crystal **IV** was in good agreement with the experimental ones [39]. For crystal **II**, the "theoretical" shape is characterized by two additional pairs of faces [(011) and (101)] when compared to the experimental crystal shape. Most probably, the formation of these faces was suppressed by the experimental conditions of crystal growth. For compound **VII** we were not able to grow crystals suitable for experimental habit investigations; thus, only those results of crystal habit modeling are presented (Fig. 7).

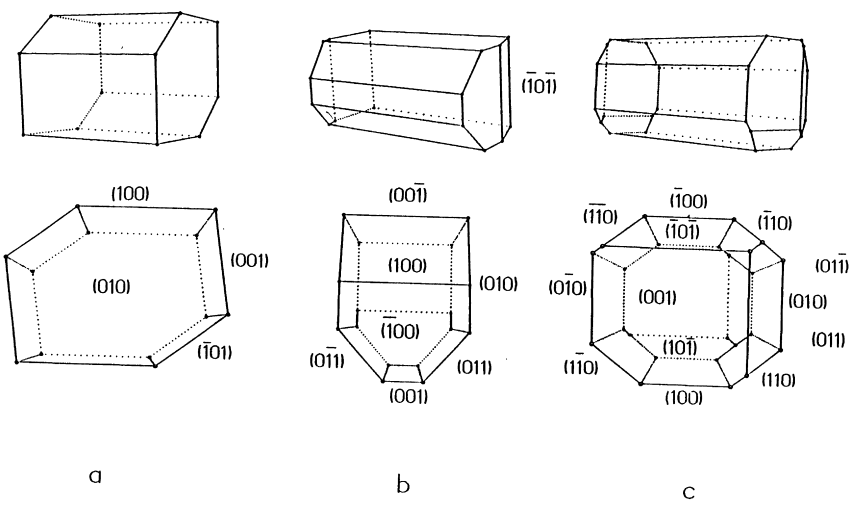

Fig. 7. Calculated crystal habit for acentric crystals: (a) **IV**; (b) **II**; (c) **VII**.

The energies of the crystal layers are listed in Table 8. This characteristic is important for the prediction of the possibility of organic film formation with a desirable orientation.

The results of the NLO investigations of crystal **IV** [39] showed two directions of phase matching for second harmonic generation: type I with 30° inclination to the (100) face, and type II with 15° inclination to the (1 0 −1) face. The choice of a special solvent or substrate could change the correlation between faces in a desirable direction. The knowledge of crystal shape and preferable crystallographic directions for SGH can be very useful for cutting the crystal for device manufacturing.

4. Conclusions

Two compounds with promising NLO properties were found from a search for molecules with molecular shape resembling the known NLO compound *o*-methoxydicyanovinybenzene (DIVA), based on molecular modeling and by screening CSD. The NLO activity of these compounds was determined to be related to the acentric molecular packing mode in the crystal. Using quantum chemical calculations for characterization of intramolecular electron density distributions, we were able to explain on a qualitative basis the presence of short contacts and the character of the molecular packing in the compounds studied. In addition, we were able to determine the influence of the packing forces on the conformation of the molecules of the series. We were also able to model crystal habit using X-ray data on the crystal structure. The latter data might be very important in using the investigated compounds for practical applications.

Supporting information available: Tables of the X-ray structure determination summary, tables of the non-hydrogen atom coordinates and their equivalent displacement parameters, bond lengths, bond angles, anisotropy displacement parameters for non-hydrogen atoms, hydrogen atoms coordinates, and their isotropic displacement parameters. Ordering information is given on any masthead page.

Supplementary data relating to this article are deposited with the B.L.L.D. as Supplementary Publication No. SUP26623.

Acknowledgements

The authors are grateful for the financial support provided by NASA, NSF, and AFOSR for the present investigation through the following grants: NASA cooperative agreements NCC8-71 and NCC8-144; NASA Alliance for Non-linear Optics (NAG5-6532); NSF Center for Theoretical Studies of Physical Systems (HRD-9450386), AFOSR Grant (F49620-97-1-0256).

References

[1] J. Zyss (Ed.), Molecular Nonlinear Optics: Materials, Physics, and Devices Academic Press/Harcourt Brace and Jovanovich, New York, 1994.
[2] D.R. Kanis, M.A. Ratner, T.J. Marks, Chem. Rev. 94 (1994) 195.
[3] Y. Itoh, K. Oono, M. Isogai, A. Kakuta, Mol. Cryst. Liq. Cryst. 179 (1989) 259.
[4] Y. Itoh, K. Oono, M. Isogai, A. Kakuta, SPIE Nonlinear Opt. Mater. 1017 (1988) 127.
[5] M.Yu. Antipin, T.A. Barr, B. Cardelino, R.D. Clark, C.E. Moore, T. Myers, B. Penn, M. Romero, M. Sangadasa, T.V. Timofeeva, J. Phys. Chem. 101 (1997) 2770.
[6] V.N. Nesterov, T.V. Timofeeva, G. Duerksen, R.D. Clark, J. Mol. Struct. 444 (1998) 135.
[7] M.Yu. Antipin, R.D. Clark, V.N. Nesterov, M. Sangadasa, T.V. Timofeeva, K.A. Lyssenko, Mol. Cryst. Liquid Cryst. 313 (1998) 85.
[8] A. Gavezzotti, C. Filippini, J. Phys. Chem. 98 (1994) 4831.
[9] A. Gavezzotti, C. Filippini, J. Am. Chem. Soc. 118 (1996) 7153.
[10] M.Yu. Antipin, T.V. Timofeeva, R.D. Clark, V.N. Nesterov, M. Sanghadasa, L. Romero, M. Romero, B. Penn, J. Phys. Chem. A 102 (1998) 7222.
[11] G. Jones, Organic Reactions, 15, Wiley, New York, 1967 p. 204.
[12] F. Freeman, Chem. Rev. 69 (1969) 591.
[13] A.J. Fatiadi, Synthesis (1978) 165.
[14] F.H. Allen, O. Kennard, Chem. Design Automation News 8 (1993) 31.
[15] Y. Delugeard, Cryst. Struct. Comm. 4 (1975) 289.
[16] GAUSS94W: Gaussian-94, Rev. A1, Gaussian, Inc., Pittsburg, PA, 1995.
[17] N.L. Allinger, Y.H. Yuh, J.-H. Lii, J. Am. Chem. Soc. 111 (1989) 8551.
[18] J.-H. Lii, N.L. Allinger, J. Am. Chem. Soc. 111 (1989) 8566.
[19] M.J.S. Dewar, J.J.P. Stewart, Chem. Phys. Lett. 111 (1984) 416.
[20] H.A. Kurtz, J.J.P. Stewart, K.M. Dieter, J. Comput. Chem. 11 (1990) 82.
[21] B.H. Cardelino, C.E. Moore, R.E. Stickel, J. Phys. Chem. 95 (1991) 8645.

[22] B.H. Cardelino, C.E. Moore, D.O. Frazier, J. Phys. Chem. A 101 (1997) 2207.
[23] QCPE; MOPAC, Quantum Chemistry Program Exchange, Version 6, 1990.
[24] Z.J. Berkovitch-Yellin, J Am. Chem. Soc. 107 (1985) 8239.
[25] G. Clydesdale, K.J. Roberts, R. Docherty, J. Cryst. Growth 166 (1986) 78.
[26] V.I. Shil'nikov, Kristallografia 39 (1994) 647.
[27] D.E. Williams, S.R. Cox, Acta Crystallogr. B 40 (1984) 404.
[28] K.D. Singer, J.E. Sohn, L.A. King, H.M. Gordon, H.E. Katzand, C.W. Dirk, J. Opt. Soc. Am B 6 (1989) 1339.
[29] B.F. Levine, C.G. Bethea, J. Chem. Phys. 63 (1975) 2666.
[30] K.N. Bhat, M. Aggarwal, B.H. Cardelino, C.E. Moore, B. Penn, D. Frazier, M. Sanghadasa, T.A. Barr, Comput. Mater. Sci. 8 (1997) 309.
[31] T. Uemiya, N. Uenishi, S. Umegaki, J. Appl. Phys. 73 (1993) 12.
[32] M. Sanghadasa, T.A. Barr, D.A. Gregory, Optical Society of America, Annual Meeting, Albuquerque, NM, 20–25 September 1992.
[33] M. Sanghadasa, T.A. Barr, D. Clomenil, Yufeng Tong, K. Bhat, R.D. Clark, B.G. Penn, in: C.M. Lawson (Ed.), Nonlinear Optical Liquids, Proc. SPIE, 2853 (1996) 37.
[34] J. Jerphagnon, S.K. Kurtz, J. Appl. Phys. 41 (1970) 1667.
[35] M.M. Choy, R.L. Byer, Phys. Rev. B 14 (1976) 1693.
[36] L.C. Groenen, W. Verboom, W.H.N. Nijhuis, D.N. Reinhoudt, G.J. van Hammel, D. Feil, Tetrahedron 44 (1988) 4637.
[37] G. Mignani, M. Barzouskas, J. Zyss, G. Soula, F. Balegroune, D. Grandjean, D. Josse, Organometallics 10 (1991) 3660.
[38] A.P. Krukonis, J. Silverman, N.F. Yannoni, Cryst. Struct. Commun. 3 (1974) 233.
[39] T. Wada, G.H. Grossman, S. Yamada, A. Yamada, A.F. Garito, H. Sasabe, Mater. Res. Soc. Symp. Proc. 173 (1990) 519.
[40] P.A. D'Agostino, L.R. Provost, J. Chromatogr. A 695 (1995) 65.